Journal of Heat and Mass Transfer Research

Journal homepage: https://jhmtr.semnan.ac.ir

Semnan University

ISSN: 2383-3068

Research Article

Cooling Performance Enhancing by Employing Hybrid Pin-Blade Fin Geometry with Constant Weight for Prismatic Lithium-Ion Batteries

Somayeh Jalalichaleshtori , Ghanbar Ali Sheikhzadeh *

Faculty of Mechanical Engineering, University of Kashan, Iran

ARTICLE INFO

Article history:

Received: 2024-11-25

Revised: 2025-06-10

Accepted: 2025-06-15

Keywords:

Hybrid fin architecture;

Hydraulic efficiency;

Prismatic lithium-ion battery;

Cold plate;

Battery thermal management system (BTMS);

Computational fluid dynamics (CFD).

ABSTRACT

This research introduces a novel hybrid pin-blade fin architecture for lithium-ion battery thermal management systems, strategically integrating complementary fin geometries to overcome the traditional thermal-hydraulic performance trade-off. Through comprehensive 3D CFD simulations, the hybrid design achieves a remarkable dual improvement: maintaining battery temperatures below 21.5°C during 5C discharge (1°C lower than conventional designs) while reducing pressure drop by 30% compared to equivalent pin-fin configurations. The investigation reveals that smaller pin diameters (2.5 mm) provide superior thermal performance, while higher blade angles (80°) significantly reduce hydraulic resistance. By combining these optimal features, the hybrid architecture delivers exceptional cooling efficiency while requiring 7% less aluminum and 66% less coolant than benchmark designs. Quantitative analysis shows that reducing pin diameters from 10 mm to 2.5 mm decreases maximum battery temperature by 0.3°C, while optimizing blade orientation angles can reduce pressure drop by up to 65 Pa at 0.2 l/min flow rate. The innovative cooling plate achieves rapid thermal stabilization within 150 seconds and sustains temperature uniformity across the battery surface. This breakthrough approach resolves the long-standing dilemma between thermal regulation and hydraulic penalties in battery cooling systems, establishing a new standard for high-performance, material-efficient thermal management in electric vehicle applications.

1. Introduction

The transportation sector, particularly the automotive industry, represents a major contributor to global air pollution and energy consumption. New energy vehicles have gained substantial market acceptance due to their superior energy efficiency, reduced noise generation, and lower emissions. These include battery-based hybrid electric vehicles (HEVs), which combine internal combustion engines with electric motors, and purely battery-driven electric vehicles (EVs) [1,2]. Lithium-ion batteries (LIBs) have become the predominant power source for clean energy vehicles due to their environmental compatibility, high energy density, extended lifecycle, and exceptional specific energy [3]. Individual LIB cells cannot generate sufficient current and voltage for most electric systems, necessitating battery packs arranged in parallel and series configurations to power applications ranging from renewable energy storage to electric vehicles. The design of these packs requires careful consideration of

* **Corresponding author.**
E-mail address: sheikhz@kashanu.ac.ir

Cite this article as:
Jalalichaleshtori, S. and Sheikhzadeh, G.A., 2026. Cooling Performance Enhancing by Employing Hybrid Pin-Blade Fin Geometry with Constant Weight for Prismatic Lithium-Ion Batteries. *Journal of Heat and Mass Transfer Research*, 13(2), pp. 159-174.
https://doi.org/10.22075/JHMTR.2025.36024.1645

safety and operational longevity [4]. LIBs face significant thermal challenges, particularly at extreme temperatures (below -20°C or above 50°C), where electrochemical performance deteriorates, leading to electrolyte crystallization, reduced lifespan, and potential thermal runaway [5,6]. Maintaining batteries within a safe operating range (25-40°C) during charge-discharge cycles is essential to prevent electrical imbalances between cells and preserve pack functionality [7]. Multiple studies have demonstrated that thermal runaway can lead to catastrophic battery fires and explosions [8].

Various battery thermal management (BTM) approaches have been developed, including phase change materials (PCMs), liquid cooling, and air-cooling systems. While PCMs offer excellent heat absorption during phase transitions, their effectiveness is limited during multiple daily charge-discharge cycles [9,10]. They also require supplementary cooling at high temperatures and are vulnerable to active loading conditions and adverse environments [11]. Air cooling systems suffer from low heat transfer coefficients and restricted airflow pathways [12], whereas liquid cooling offers superior temperature homogeneity due to higher density, enhanced specific heat capacity, and better thermal conductivity [13]. Most automotive manufacturers have adopted liquid or air-cooling approaches based on cooling capacity, cost considerations, compactness requirements, and anticipated operating conditions [14].

Wang et al. identified liquid cooling as the most cost-effective and efficient medium for LIB module thermal management when analyzing heat pipe performance [15]. Wu et al. demonstrated that variable heat transfer path (VHTP) cooling plates reduced temperature variation across battery surfaces by 22.7-25.4% across various operating conditions [16]. Deng et al. have established that a coolant mass flow rate of 1 $g{\cdot}s^{-1}$ provides optimal thermal dissipation, with maximum battery module temperatures of 32.17°C and 27.67°C for 5C and 3C discharge rates, respectively. Strategic positioning of cooling channels in battery modules significantly enhances heat dissipation performance and temperature distribution homogeneity [17]. Flow direction and inlet/outlet positioning substantially impact cooling plate power consumption and temperature distribution. While increased fluid flow minimally affects temperature distribution patterns, it effectively reduces maximum temperature elevation within cell packs [18]. Comparison of microchannel configurations under varying conditions showed that wavy-walled designs reduced maximum temperature by 4-6°C depending on wave amplitude, while metal foam-embedded microchannels achieved a 14°C reduction compared to straight configurations while maintaining desirable temperature variation [19]. Sevilgen et al.'s experimental and numerical assessment of lithium titanate oxide battery packs demonstrated that optimized cold plate designs achieved a 45% reduction in maximum temperature compared to conventional designs under identical operating conditions [20]. Zhang et al. developed bionic leaf-vein structured cooling channels that reduced maximum temperatures by 1.06°C to approximately 33°C while decreasing pressure drop by 40.03% and standard temperature difference by 8.98% [21]. Separate investigations of rib-grooved liquid-cooled plates showed lower maximum battery temperatures (by 0.74°C) compared to conventional straight-channel designs, albeit with increased pressure drop (55.37Pa) [22]. Li et al. evaluated four distinct liquid-cooled microchannel configurations for a 35V battery module comprising 12 LiFePO4 pouch cells. Their optimal design maintained maximum temperatures around 30°C with temperature differentials below 5°C across various discharge rates. This emphasizes the importance of appropriate coolant flow rate selection to balance temperature control and cooling efficiency [23]. Rao et al. demonstrated that wedge-shaped microchannel cold plates provided excellent temperature homogeneity, with side-cooling approaches reducing temperature variation by up to 35.71% compared to front cooling. A flow rate of $1{\times}10^{-4}$ kg/s maintained temperatures below 45°C at 3.5C discharge rates, while branching designs reduced maximum temperature variation from 7.27°C to 4.67°C [24].

Recent topology optimization research for liquid cooling plates has focused on enhancing thermal performance through optimized inlet/outlet positioning [25]. Monika et al. proposed a cold plate featuring five 4 mm-wide mini-channels in parallel configuration, with water entering at 25°C and 0.003 $kg{\cdot}s^{-1}$, demonstrating uniform longitudinal heat distribution [26]. Two-dimensional topology optimization methodologies have produced cooling plates in various configurations, including dual-exit and entrance arrangements. These studies showed that optimized structures achieve superior heat dissipation under low-flow conditions, with branch patterns evolving from concentrated solid zones to distributed networks as flow parameters change [27]. Bionic cooling plates modeled after plantain leaf vein structures have demonstrated that smaller branch angles and greater branch quantities enhance cooling efficiency. At 1g/s coolant flow with 3C discharge rates, these designs maintained maximum

temperature variation and peak temperature at 4.95°C and 31.75°C respectively, providing excellent temperature homogeneity with minimal pressure drop [28]. Regarding the impact of flow patterns and solid block contact surfaces on the thermal management of electric vehicle lithium-ion batteries, parallel flow can lead to higher temperatures near the inlet, while counter-flow increases side cell maximum temperatures. Additionally, increasing the contact surface area resulted in a substantial weight reduction of around 28.5% for solid blocks [29].

Building upon these foundations, this study introduces a revolutionary hybrid pin-blade fin architecture that fundamentally transforms thermal management for prismatic lithium-ion batteries. This groundbreaking approach strategically integrates complementary fin geometries to achieve what previous designs considered mutually exclusive: superior thermal regulation with minimal hydraulic penalties. Through comprehensive 3D coupled CFD simulations, the investigation quantitatively demonstrates that the hybrid architecture resolves the long-standing thermal-hydraulic trade-off dilemma while reducing material requirements. The findings advance the fundamental understanding of complex flow structures in multi-geometry cooling plates and provide practical design guidelines for next-generation battery thermal management systems, with direct implications for extending battery lifespan and enhancing electric vehicle performance.

2. Materials and Methods

2.1. Cooling Plate Design

The cooling plate structure is determined by the properties of commercial pouch and prismatic LIB cells. This paper presents cooling plate design concepts applicable to various pouch and prismatic LIB configurations. The cooling plate design process prioritizes several critical factors:

(a). minimizing BTMS weight and dimensional footprint,

(b). reducing coolant pressure drop within the cooling plate,

(c). maximizing heat dissipation from LIBs to prevent thermal propagation between adjacent cells in battery modules,

(d). maintaining LIB cell temperatures within manufacturer-specified ranges during normal operation.

Minimizing the coolant pressure drop serves multiple practical purposes, including reducing coolant leakage risk, lower operating pressure requirements, decreased pump energy consumption, and smaller pump dimensions.

The cooling plate dimensions, material properties, coolant medium characteristics, and LIB specifications are detailed in Table 1. The coolant path thickness in the cooling plate structure is maintained at 2 mm (3 mm less than the design in Ref. [4]), with cross-sectional dimensions of 160 mm width and 225 mm height. The cooling plate is fabricated from aluminum 6063 with a 0.5 mm sheet thickness, selected for its exceptional thermal conductivity, superior strength-to-weight ratio, and lightweight characteristics, properties essential for efficient thermal management in battery applications.

Table 1. Material properties used in simulation [4]

Parameter	LIB	60% Ethylene glycol in water @20 °C	Aluminum 6063
Heat capacity (Cp), [J/(kg·K)]	1400	3216	900
Density (ρ), [kg/m^3]	2100	1090	2700
Thermal conductivity (k), [W/(m·K)]	26.92 (x & y axis) 1.68 (z axis)	0.375	201
Dynamic viscosity (μ). [Pa·s]	-	0.0038	-

A sandwich configuration (plate-battery-plate) has been implemented to maximize thermal contact with the LIB cells, as illustrated in Fig. 1a.

The engineered cooling plates (Fig. 1) incorporate strategic fin geometries to enhance effective heat transfer surface area between coolant and plate, thereby promoting temperature homogeneity across the battery surface. This investigation focuses on two distinct cooling plate architectures: pin fin structures and blade fin configurations, each arranged in various geometric orientations. To establish meaningful comparative analysis, the aluminum sheet mass is maintained as a constant parameter across all design variations, while modifying fin geometry, quantity, and arrangement.

For pin fin configurations (Fig. 1c), three discrete diameter specifications (2.5 mm, 5 mm, and 10 mm) are systematically evaluated to optimize thermal performance.

The blade fin designs (Figure 1d) are characterized by varied angular orientations (20°, 30°, 45°, 60°, and 80°) to determine optimal flow patterns. These specific geometric configurations were selected based on prior research establishing their superior thermal distribution characteristics and minimal pressure drop performance in cooling plate applications [4].

The pin structures serve multiple critical functions, effectively reducing temperature gradients within both the cooling plate and battery while simultaneously facilitating coolant flow throughout the system with minimal pressure drop. Operating as miniaturized heat sinks, these pins significantly expand the effective heat transfer surface area within the cooling plate. Their spatial distribution is precisely calculated to ensure optimal coolant dispersion across the entire plate surface. Following comprehensive simulation of both architectural models, with a particular emphasis on pressure drop metrics and maximum temperature profiles, a hybrid fin configuration has been developed. This optimized design integrates elements from both pin and blade geometries to produce a novel cooling plate architecture that achieves minimum temperature gradients while maintaining acceptable low pressure drop characteristics. The basis for selecting the fin geometry is inspired by plate heat exchangers, which use circular and blade fins according to the exchanger geometry. Since the volume of aluminum used for the fins is considered constant, the temperature distribution is non-uniform for circular fins larger than 10 mm, and smaller than 2.5 mm, the pressure drop in the plate increases more than the results obtained, which is not desirable. Furthermore, to select fin blade angles, cooling plate conditions were investigated by increasing the angle by 10 degrees relative to the horizontal axis, and the results were almost similar for angles smaller and larger than this range. The 45-degree and 50-degree angles obtained almost the same results as in the initial study. Since the 45-degree angle is more frequently studied in plate heat exchanger designs, and was not entirely optimal in the research conducted, it was included in this analysis.

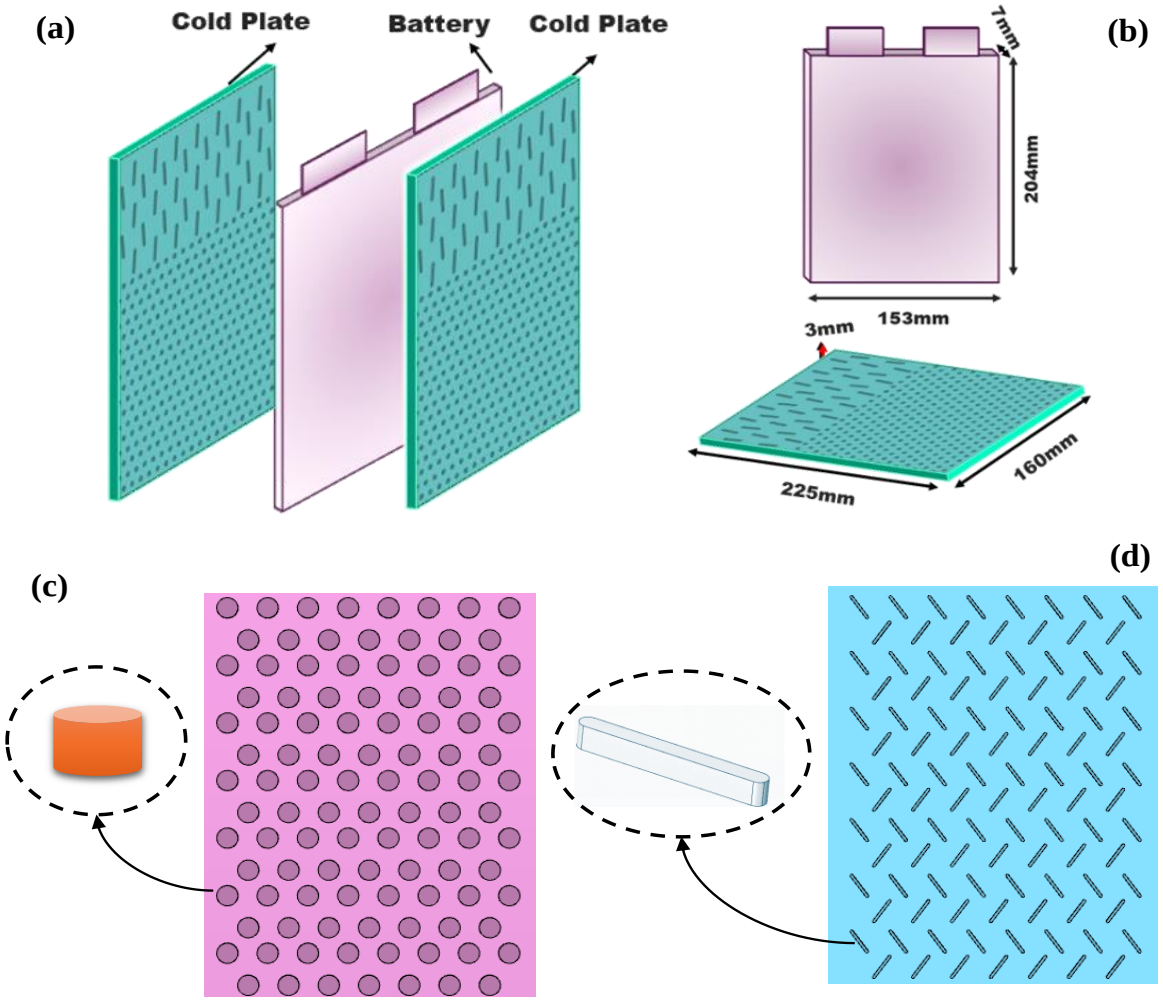

Fig. 1. Cooling system design and components: (a) Battery and cold plate arrangement showing sandwiched configuration, (b) Dimensions of battery (153mm × 204mm × 7mm) and cold plate (160mm × 225mm × 3mm), (c) Pin fin cold plate design showing cylindrical protrusion pattern, and (d) Blade fin cold plate design showing angled fin arrangement

2.2. CFD Modelling

The performance of the proposed cooling plate designs was evaluated through rigorous CFD simulations and thermal modeling. For this analysis, the LIB was modelled as a volumetric heat generation source operating under standard conditions. A comprehensive three-dimensional, coupled heat transfer model was developed using COMSOL Multiphysics to accurately represent the complex thermal interactions between the battery cells, cooling plates, and coolant flow. This sophisticated simulation framework incorporates:

- Conjugate heat transfer in the solid domains (LIB and aluminum cooling plates)
- Non-isothermal fluid flow dynamics in the liquid domain (coolant)
- Thermal interface conditions at solid-fluid boundaries
- Temperature-dependent material properties

The simulation parameters were calibrated using experimental data obtained from direct measurements of the heat generation within lithium-ion batteries. Following the methodology established in [30], volumetric heat generation rates (W/m^3) were mapped across seven discrete regions of the battery during both 1C charging and 5C discharging cycles. This spatially-resolved heat generation profile was captured using strategically positioned heat flux sensors, providing a high-fidelity thermal generation pattern that served as the foundation for our computational model. The validated computational framework enabled comprehensive evaluation of thermal gradients, maximum temperatures, pressure drops, and flow patterns across the various cooling plate geometries, allowing for systematic optimization of thermal management system design.

3. Mathematical Model Description

3.1. Battery Electrochemical Modeling

The lithium-ion battery model incorporates a comprehensive framework describing charge transport and mass conservation phenomena. For a static binary 1:1 electrolyte system consisting of lithium cations (Li^+) and corresponding anions (An^-), the governing equations for the battery separator are expressed as [31]:

$$\frac{\partial(\varepsilon_l c_l)}{\partial t} + \nabla \cdot (J_l) = R_l \tag{1}$$

$$\nabla \cdot i_l = Q_l \tag{2}$$

$$J_l = -D_{l,eff}\nabla c_l + \frac{i_l t_+}{F} \tag{3}$$

$$i_l = -\sigma_{l,eff}\nabla\phi_l + \frac{2\sigma_{l,eff}RT}{F}\left(1 + \frac{\partial \ln f}{\partial \ln c_l}\right)(1 - t_+)\nabla \ln c_l \tag{4}$$

where ε_l represents the electrolyte volume fraction, c_l denotes the electrolyte salt concentration, R_l signifies the total lithium-ion source term in the electrolyte, and Q_l represents an arbitrary electrolyte current source. The lithium-ion transport number is denoted by t+, while F represents Faraday's constant (96,485 C·mol^{-1}), R is the universal gas constant, and T denotes the temperature. The salt activity coefficient is represented by f, while the effective electrolyte mass diffusivity $D_{l,eff}$ and conductivity $\sigma_{l,eff}$ are defined as:

$$D_{l,eff} = \varepsilon_l^{1.5} D_l \tag{5}$$

$$\sigma_{l,eff} = \varepsilon_l^{1.5} \sigma_l \tag{6}$$

For porous electrodes, the governing equations are modified to account for the complex microstructure and electrochemical reactions:

$$\frac{\partial(\varepsilon_l c_l)}{\partial t} + \nabla \cdot (J_l) = -\sum_m v_{Li^+,m} i_{v,m} - \frac{v_{Li^+,m} i_{v,m}}{nF} + R_{l,src} \tag{7}$$

$$\nabla \cdot i_l = i_{v,total} + Q_l \tag{8}$$

$$\nabla \cdot i_s = -i_{v,total} + Q_s \tag{9}$$

$$J_l = -D_{l,eff}\nabla c_l + \frac{i_l t_+}{F} \tag{10}$$

$$i_l = -\sigma_{l,eff}\nabla\phi_l + \frac{2\sigma_{l,eff}RT}{F}\left(1 + \frac{\partial \ln f}{\partial \ln c_l}\right)(1 - t_+)\nabla \ln c_l \tag{11}$$

$$i_s = -\sigma_{s,eff}\nabla\phi_s \tag{12}$$

In Eqs. (7)-(12), σ_s denotes the electric conductivity in the solid phase, $\Delta\phi_s$ represents the potential drop across the solid-electrolyte interface (SEI) layer, c_s signifies the lithium concentration in the electrode particles, and itot represents the total electrochemical current. Porous electrodes have effective transport parameters defined by:

$$D_{l,eff} = f_l D_l \tag{13}$$

$$\sigma_{l,eff} = f_l \sigma_l \quad (14)$$

$$\sigma_{s,eff} = \sigma_s \quad (15)$$

These equations collectively capture the electrochemical processes occurring within the battery, including lithium intercalation/deintercalation, electrolyte transport, and charge transfer reactions, which ultimately govern the battery's thermal behavior during operation. The model accounts for the complex interplay between concentration gradients, potential differences, and electrochemical kinetics that determine the battery's performance and heat generation characteristics under various operating conditions.

3.2. Coolant Flow Equations

To obtain the velocity distribution of the coolant within the heat exchanger, it is necessary to determine the type of flow regime. Based on this regime, laminar or turbulent flow models should be selected. Typically, the flow of coolant inside heat exchangers for BTMSs exhibits laminar characteristics. To determine whether the cooling flow is laminar or turbulent within the cooling plate during both normal operation and thermal runaway conditions, the Reynolds number (*Re*) is calculated using the following equation [4]:

$$Re = \frac{\rho_c u_c D_h}{\mu_c} \quad (16)$$

where ρ_c represents the coolant density in the cooling plate [kg/m^3], u_c signifies the average coolant velocity [m/s], *Dh* denotes the hydraulic diameter [m], and μc corresponds to the coolant dynamic viscosity [Pa·s]. The average coolant velocity (u_c) is determined from:

$$u_c = \frac{\dot{V}_c}{\delta_c w} \quad (17)$$

where $\dot{V}_c$ indicates the volumetric coolant flow rate [m^3/s], δ_c relates to the thickness of coolant flow path in the cooling plate [m], and w characterizes the width of coolant flow path [m]. The hydraulic diameter is calculated as follows:

$$D_h = \frac{2\delta_c w}{(\delta_c + w)} \quad (18)$$

The coolant used is 60% ethylene glycol (by volume) in water, selected for its excellent anti-freezing properties, which are critical for operation in cold climatic conditions. For the 0.6 l/min coolant flow rate, the Reynolds number is calculated to be 35.4. This value indicates a laminar flow regime for coolant flow rates of 0.6, 0.3, and 0.2 l/min.

The transient behavior of coolant flow, considered as an incompressible fluid, is characterized by fundamental conservation principles for mass (continuity) and momentum, which are mathematically expressed as follows [4]:

$$\rho_c \nabla \cdot u_c = 0 \quad (19)$$

$$\rho_c \frac{\partial u_c}{\partial t} + \rho_c (u_c \cdot \nabla) u_c = \nabla p + \mu_c \nabla^2 u_c + \rho g \quad (20)$$

In Eq. (20), p signifies the fluid pressure [Pa], while g represents the gravitational acceleration acting on the system [m/s^2].

3.3. System Energy Balance Equations

To attain temperature distribution throughout the battery and cooling system, and to effectively manage thermal energy within the package, energy balanced equations must be established for all system components. These equations account for both conductive heat transfer through the solid domains and convective heat transfer between battery components and coolant. The governing energy equation for the battery, incorporating the heat generated within the battery, can be written as follows:

$$\frac{\partial}{\partial t}\left(\rho_b C_{p,b} T_b\right) = \nabla \cdot (k_b \nabla T_b) + \dot{Q}_{gen,b} - \dot{Q}_{b,cp} \quad (21)$$

In Eq. (21), ρ_b, $C_{p,b}$, and k_b refer to the density, specific heat capacity, and thermal conductivity of the LIB, respectively. The temperature gradient is denoted by ∇T_b, while $\dot{Q}_{gen,b}$ represents the rate of heat generation in the LIB per unit volume, which is estimated from battery electrochemical modeling. Additionally, $\dot{Q}_{b,cp}$ indicates the heat removal rate per unit volume from the LIB via the cooling plate.

Since the prismatic LIB consists of various coupled layers, the density and specific heat capacity of the LIB can be determined from Eq. (22) and Eq. (23), respectively [32]. In these equations, δ_i, $\rho_{b,i}$, and $C_{p,i}$ refer to the thickness, density, and specific heat capacity of the component layer i of the LIB. The parameter δ denotes the overall LIB thickness.

$$\rho_b = \frac{1}{\delta} \sum_i \delta_i \rho_{b,i} \quad (22)$$

$$C_{p,b} = \frac{1}{\delta} \sum_i \delta_i C_{pb,i} \quad (23)$$

Heat transfer inside LIBs exhibits an anisotropic behavior due to the varying thicknesses and thermal conductivities of the constituent layers. Heat flow direction significantly influences thermal conductivity calculations. The thermal conductivity of the LIB along the x and y axes can be determined using the parallel arrangement of layers in the LIB, as expressed in Eq.(24) [31]:

$$k_x = k_y = \frac{1}{\delta}\sum_i \delta_i k_i \tag{24}$$

where k_i represents the thermal conductivity of layer i inside the LIB. It should be noted that the LIB thermal conductivity in the z-axis direction is determined by the series arrangement of layers in the LIB, as obtained by Eq. (25) [31].

$$k_z = \frac{\delta}{\sum_i \frac{\delta_i}{k_i}} \tag{25}$$

The temperature distribution for the cooling plate based on different configurations and designs is obtained by solving the governing energy balance equation expressed in Eq. 9 as follows [4].

$$\frac{\partial}{\partial t}\left(\rho_{cp} C_{p,cp} T_{cp}\right) = \nabla \cdot \left(k_{cp} \nabla T_{cp}\right) + \dot{Q}_{b,cp} - \dot{Q}_{cp,c} \tag{26}$$

where ρ_{cp}, $C_{p,cp}$, and k_{cp} represent the density, specific heat capacity, and thermal conductivity of the cooling plate, respectively. $\dot{Q}_{cp,c}$ and $\dot{Q}_{b,cp}$ determine the heat transfer rate from the cooling plate to the coolant and from the battery to the cooling plate per unit volume, respectively.

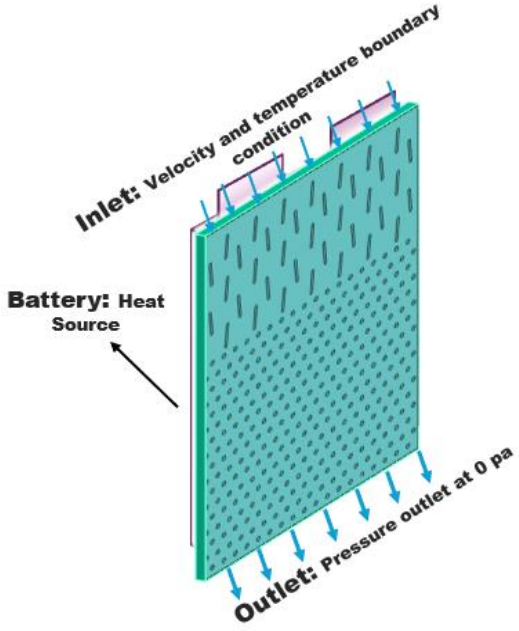

Fig. 2. Schematic representation of the computational domain showing the symmetry-reduced half-battery model with applied boundary conditions

4. Initial and Boundary Conditions

At the simulation start point, all system components maintain thermal equilibrium under ambient conditions. The battery electrochemical domain initiates with zero potential in both electrodes and electrolytes, while the electrolyte preserves its initial concentration. The fluid domain began in a quiescent state, with static coolant and atmospheric pressure throughout. Due to the symmetry of the xz-plane, the computational domain was reduced to half of the battery-cooling plate assembly to enhance computational efficiency. As illustrated in **Fig. 2**, the 3D model incorporates a prismatic lithium-ion battery cell with dimensions of 3.5 mm thickness, 153 mm width, and 204 mm height. The cooling plate, positioned in direct thermal contact with the battery surface, has dimensions of 1.5 mm thickness, 160 mm width, and 225 mm height.

4.1. Thermal Management System Boundaries

The coolant circuit boundaries are constrained by:

- Inlet condition: Prescribed mass flow rate and temperature
- Outlet condition: Zero-gauge pressure (atmospheric reference)
- Heat transfer at outlet: Free outflow condition
- External surfaces: Natural convection from the ambient environment

These boundary conditions collectively establish a well-posed mathematical framework that captures the coupled electrochemical and thermal behavior of the battery system during operation, allowing for accurate prediction of temperature distributions and cooling performance across various discharge rates and operational scenarios.

5. Mesh Independence Analysis and Model Validation

5.1. Grid Independence Study

A comprehensive mesh independence analysis was conducted to ensure numerical results reliability and accuracy. The computational domain was discretized using unstructured tetrahedral elements with enhanced boundary layer refinement at critical interfaces, particularly at the battery-cooling plate junction where significant temperature gradients exist. As shown in **Fig. 3**, systematic mesh refinement studies were performed with

grid sizes ranging from approximately 2.5×10^5 to 3.0×10^6 elements. The maximum battery temperature ($T_{battery,max}$) was selected as the critical parameter for evaluating grid convergence. The results demonstrate that $T_{battery,max}$ decreases asymptotically with increasing mesh density, from 22.34°C at the coarsest mesh (2.5×10^5 elements) to 22.24°C at the finest mesh resolution (3.0×10^6 elements).

A reduction in $T_{battery,max}$ of approximately 0.08°C was observed when refining the mesh from 2.5×10^5 to 7.5×10^5 elements, indicating that the coarsest mesh was insufficient to capture thermal gradient accurately. However, the variation in $T_{battery,max}$ between mesh sizes of 1.5×10^6 and 3.0×10^6 elements was less than 0.01°C (approximately 0.04%), suggesting that grid independence was effectively achieved at 1.5×10^6 elements.

To balance computational efficiency with solution accuracy, a mesh resolution of 1.5×10^6 elements was selected for all subsequent simulations. This mesh density provided sufficient resolution to capture the thermal and fluid flow phenomena while maintaining a reasonable computational cost. Special attention was given to regions with high temperature gradients and complex flow patterns, with local mesh refinement applied accordingly.

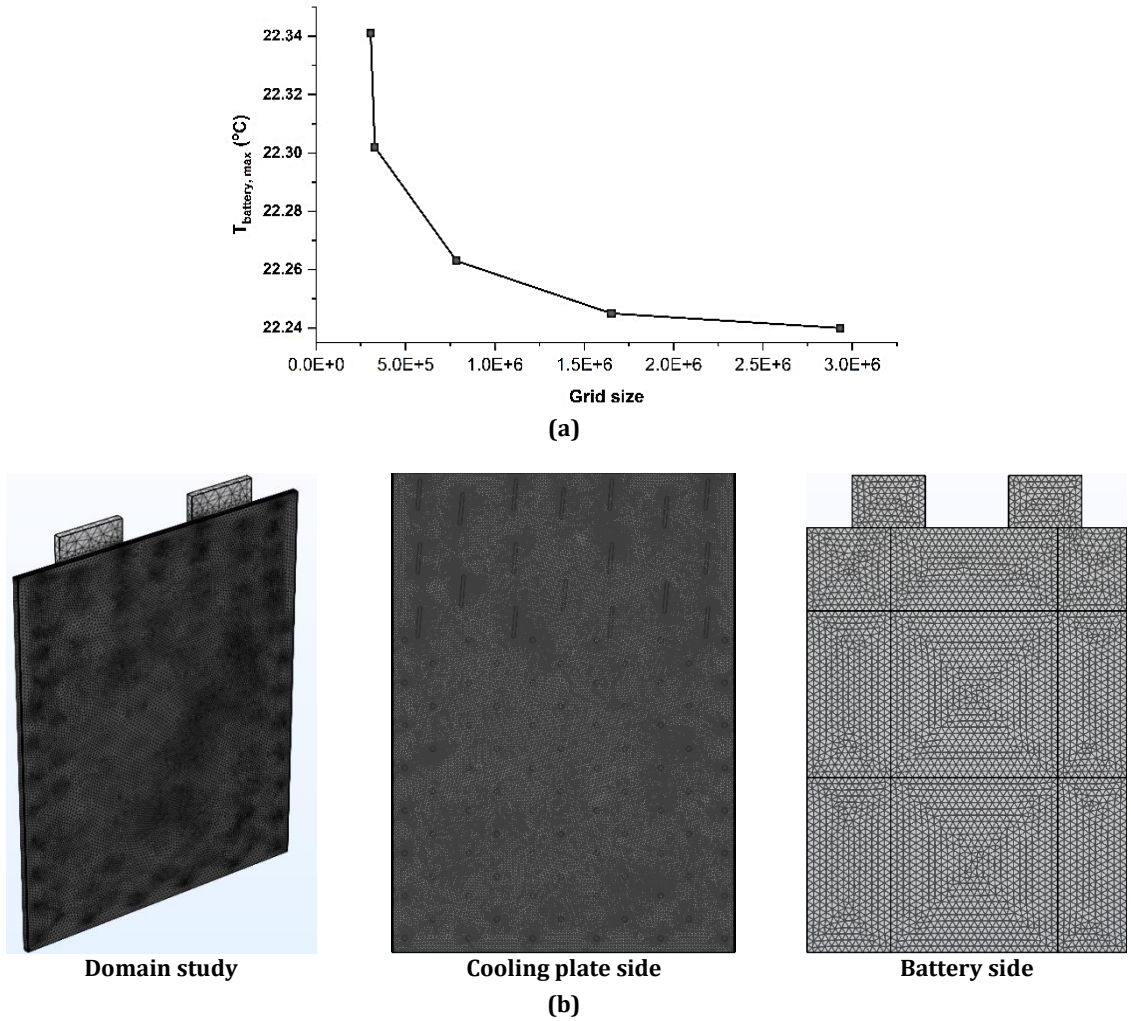

Fig. 3. (a) Grid independence study showing the relationship between maximum battery temperature and mesh resolution; (b) Mesh domain

5.2. Model Validation

The numerical model was rigorously validated against experimental data from the literature to establish confidence in its predictive capabilities. **Fig. 4** presents a comparison between the maximum battery temperature obtained from the current CFD model and the source experimental values from reference [4]. The temporal evolution of maximum battery temperature shows excellent agreement between CFD predictions and experimental measurements. Both datasets exhibit similar thermal response characteristics, with an initial rapid temperature rise followed by a gradual approach to steady-state conditions around 22.5°C after approximately 300 seconds of operation. The mean absolute deviation between

the experimental and numerical results was calculated to be 0.17°C, with a maximum discrepancy of 0.32°C occurring during the transient phase after approximately 100 seconds. The time-averaged relative error between the experimental and numerical data was 1.42%, which falls well within the acceptable range for thermal analysis of battery systems. The slight underprediction of temperatures by the CFD model during the early transient phase (0-150 seconds) can be attributed to thermal contact resistance effects that were not fully captured in the numerical model. However, the steady-state values demonstrate excellent agreement with a deviation of less than 0.1°C after 300 seconds.

Statistical analysis of the validation results yields a Pearson correlation coefficient of 0.985 between the experimental and numerical datasets, confirming the high fidelity of the computational model. The validation results demonstrate that the developed numerical model adequately captures both the transient and steady-state thermal behavior of the battery cooling system, providing a reliable foundation for subsequent parametric studies and design optimization analyses.

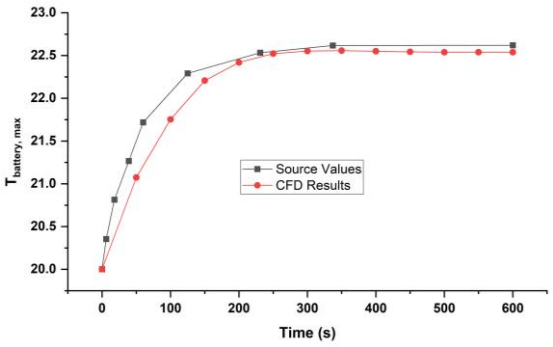

Fig. 4. Comparison of maximum battery temperature evolution over time between the present CFD simulation results (red circles) and reference experimental data (black squares) from [4]

6. Results and Discussion

A comprehensive parametric investigation was conducted to evaluate modified cooling plate designs incorporating various enhancement structures for a pouch-type lithium-ion battery during 5C discharge conditions [4]. The study examined two primary fin geometries, blade fins with different angular orientations and pin fins with varying diameters, with a constant coolant flow rate of 0.2 l/min.

6.1. Comparative Performance of Blade-Type and Pin-Type Cooling Plates

Fig. 5 and **Fig. 6** illustrate the temporal evolution of maximum battery temperature for blade-type and pin-type cooling configurations, respectively. All designs exhibit similar thermal response characteristics, with a common initial temperature of 20°C followed by a rapid temperature increase during the first 100 seconds, and eventual stabilization after approximately 200 seconds.

6.1.1. Blade-Type Fin Performance

As shown in **Fig. 5**, blade-type fin thermal performance depends on the fin orientation angle (θ). Interestingly, the fin configuration with θ = 20° exhibits the highest steady-state temperature (approximately 22.35°C), contrary to what might be expected from traditional heat transfer principles. The configurations with θ = 30° and θ = 45° demonstrate intermediate performance with steady-state temperatures around 22.3°C, while the θ = 60° design shows slightly better performance. The blade-type fin with θ = 80° achieves the lowest steady-state temperature (approximately 22.25°C), indicating superior cooling performance among blade-type configurations. This counter-intuitive relationship between fin angle and thermal performance suggests complex flow dynamics within cooling plates, where larger angles may create favorable flow patterns that enhance heat transfer.

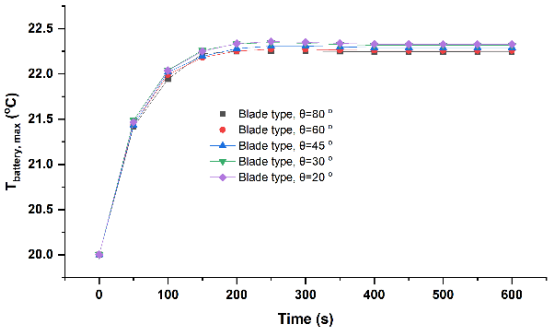

Fig. 5. Temporal evolution of maximum battery temperature during 5C discharge for blade-type cooling plates with different fin orientation angles (θ = 20°, 30°, 45°, 60°, and 80°) at a constant coolant flow rate of 0.2 l/min

6.1.2. Pin-Type Fin Performance

The pin-type fin configurations, as depicted in Fig. 6, demonstrate a clear relationship between pin diameter and thermal performance. The smallest diameter pins (D = 2.5 mm) provide the most effective cooling, maintaining the lowest steady-state temperature of approximately 22.15°C. As pin diameter increases, cooling performance progressively deteriorates, with D = 5 mm achieving an intermediate steady-state temperature of approximately 22.25°C, and D = 10 mm resulting in the highest temperature of approximately 22.45°C. This trend aligns with heat transfer principles where smaller diameter

pins provide a greater surface area-to-volume ratio, promoting enhanced convective heat transfer. Additionally, the arrangement of smaller pins likely creates more tortuous flow paths that increase turbulence and boundary layer disruption, further enhancing heat transfer coefficients.

6.1.3. Comparative Analysis

Comparing the performance of both fin types reveals that the pin-type configuration with D = 2.5 mm offers the best overall thermal management performance, achieving approximately 0.1°C lower steady-state temperature than the best blade-type design (θ = 80°). This suggests that under the examined operating conditions (5C discharge rate with 0.2 l/min coolant flow), optimized pin-fin geometries may offer marginally superior cooling efficiency. All tested configurations reach thermal equilibrium within approximately 200 seconds, indicating that the transient response characteristics are primarily influenced by the battery's inherent thermal properties rather than cooling plate design variations. The relatively modest temperature differences between configurations (maximum $\Delta T \approx 0.3$°C) suggest that while geometric optimization provides measurable benefits, all tested designs maintain battery temperatures within a narrow, operationally acceptable range during the simulated 5C discharge scenario.

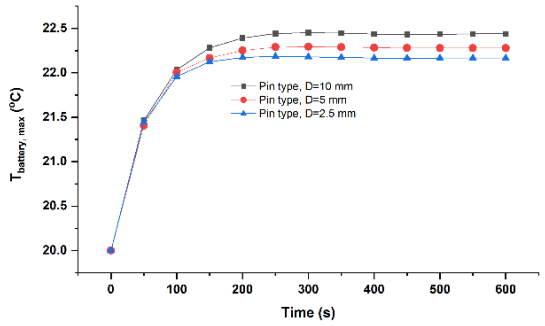

Fig. 6. Temporal evolution of maximum battery temperature during 5C discharge for pin-type cooling plates with different fin diameters (D = 2.5, 5, and 10 mm) at a constant coolant flow rate of 0.2 l/min

6.2. Impact of Pin Diameter in a Cold Plate

The effect of pin diameter on cooling performance was systematically evaluated by comparing designs with pin diameters of 2.5, 5, and 10 mm while maintaining a fixed total pin mass across all configurations. As shown in **Fig. 6**, a clear correlation exists between pin diameter and thermal management efficiency. At a coolant flow rate of 0.2 l/min with an inlet temperature of 20°C, the maximum battery temperatures reached steady-state values of approximately 22.15, 22.25, and 22.45°C for pin diameters of 2.5, 5, and 10 mm, respectively.

Fig. 7 provides a comprehensive visualization of both flow patterns (top row) and the resulting temperature distributions (bottom row) for the three pin diameter configurations at a coolant flow rate of 0.6 l/min. The velocity contours in **Fig. 7**a reveal significant differences in flow distribution.

The 10 mm configuration (left column) creates pronounced channeling with high-velocity regions (yellow-red) between the pins and substantial low-velocity zones (dark blue) in the wake regions. This non-uniform flow translates directly to the temperature distribution shown below, where significant thermal non-uniformity is evident with hot spots exceeding 21°C (red-orange regions) concentrated in the lower portions of the battery surface. The 5 mm pin configuration (center column) demonstrates notably improved flow distribution with more evenly dispersed velocity patterns. This translates to a more moderate temperature gradient across the battery surface, though some thermal non-uniformity persists in the lower region as indicated by the yellow-orange areas. The 2.5 mm pin configuration (right column) achieves the most homogeneous flow pattern with minimal wake regions and well-distributed velocity throughout the cooling plate. The resulting temperature contour shows superior thermal uniformity across the entire battery surface, with consistent cooling and a maximum temperature range of approximately 20.2-20.8°C according to the temperature scale. This represents a significant improvement in absolute temperature reduction and thermal uniformity compared to other configurations.

These visualizations conclusively demonstrate that small pin diameters provide enhanced thermal performance through two primary mechanisms: (1) increased surface area for heat exchange while maintaining the same total mass, and (2) more uniform flow distribution with reduced channeling effects that promote consistent heat removal across the entire battery surface. Despite the thermal advantages, the increased flow resistance of smaller pin configurations creates higher pressure drops across the cooling plate. This hydraulic penalty must be balanced against thermal performance gains when optimizing cooling system designs, particularly for applications with limited pumping power. Even in the best-performing 2.5 mm configuration, a slight temperature increase is still evident from top to bottom, indicating that coolant warming remains a factor as it absorbs heat throughout the flow path. These results demonstrate that pin diameter significantly impacts battery cooling

magnitude and uniformity. While smaller diameter pins (2.5 mm) offer measurable advantages in both reducing maximum temperature and improving temperature distribution, the optimal pin geometry must be determined by considering the trade-off between thermal performance, pressure drop penalties, and manufacturing constraints for practical implementation in battery thermal management systems.

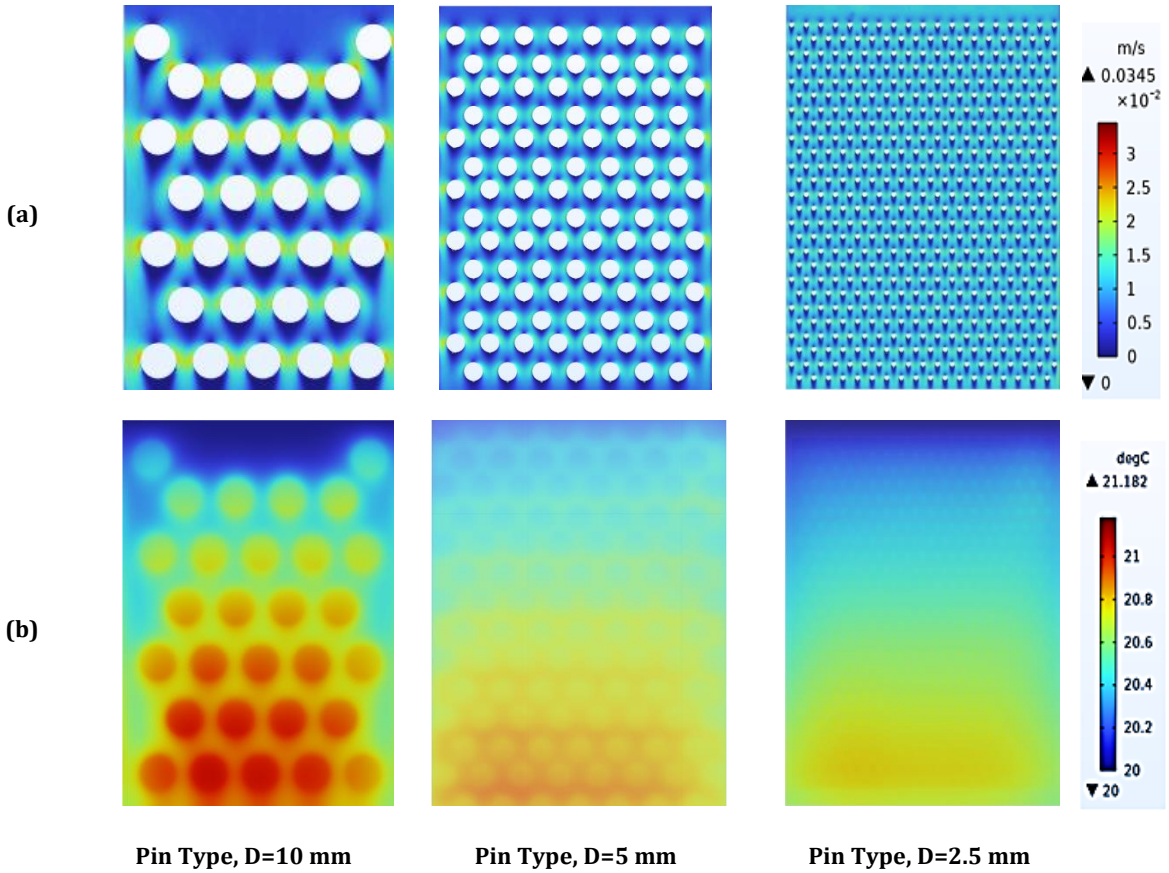

Fig. 7. Comparative analysis of pin-fin cooling plates with varying diameters (D = 10 mm, 5 mm, and 2.5 mm from left to right): (a) Top row showing velocity contours illustrating flow distribution patterns; (b) Bottom row showing corresponding temperature distributions on the battery surface with temperature scale in °C (right)

6.3. Impact of Blade Angle Fins on a Cold Plate

As illustrated in Fig. **8**, blade-shaped fins were investigated at various orientation angles (20°, 30°, 45°, 60°, and 80° relative to the x-axis direction) and compared with pin fins and a no-fin baseline at a 0.6 l/min flow rate. The temperature distribution contours reveal distinct thermal performance characteristics across all these configurations.

The top row of contours (showing 20°, 30°, and 45° blade angles) demonstrates similar thermal patterns with pronounced temperature gradients from the coolant inlet (top) to outlet (bottom). These configurations exhibit maximum temperatures of approximately 21°C in the lower regions (red-orange areas), with the 20° configuration showing slightly higher peak temperatures. The bottom row contours (60° and 80° blade angles, pin fin, and no-fin baseline) illustrate progressive thermal management capability changes. As blade angles increase in the x-axis direction (approaching 80°), both maximum and average battery temperatures decrease marginally. The 60° and 80° configurations show modestly improved temperature distributions compared to the lower angle designs, though they maintain similar overall gradient patterns. The pin fin configuration (bottom row, third image) demonstrates substantially superior thermal performance with significantly lower maximum temperatures and improved temperature uniformity compared to all blade configurations. The distinctive blue-green regions indicate temperatures between 20.2-20.6°C across much of the battery's surface, with only a small yellow region (approximately 20.8°C) near the bottom. This represents a temperature reduction of nearly 0.5°C compared to the blade fin design.

The no-fin baseline (bottom right) exhibits the poorest thermal performance with extensive red regions indicating temperatures above 21°C across much of the battery surface, confirming the necessity for enhanced cooling structures.

While the temperature differential between various blade angles is relatively modest (approximately 0.1-0.2°C), hydraulic performance varies significantly across configurations. Pressure drop measurements indicate that as blade angles increase from 20° to 80° relative to the x-axis, the pressure drop across the cooling plate decreases substantially. At a flow rate of 0.2 l/min, the pressure differential between blade fins oriented at 20° versus 80° was measured at approximately 65.04 Pa.

When maintaining equivalent fin mass across all configurations, blade fins oriented at 60° and 80° exhibit lower pressure losses compared to pin fins. However, Figure 8 clearly demonstrates pin fins provide superior thermal management despite their higher pressure drop penalty. This highlights a critical design trade-off: blade fins at higher angles (60°-80°) offer improved hydraulic efficiency with moderate thermal performance, while pin fins deliver substantially enhanced temperature control but require increased pumping power. These findings indicate that optimal fin configuration depends on specific design priorities. In applications where pumping power is severely constrained, blade fins oriented at higher angles (60°-80°) may represent a viable compromise. However, when thermal performance is the primary consideration and an adequate pumping capacity is available, pin fins clearly offer superior temperature regulation as visually evidenced by the contour visualization.

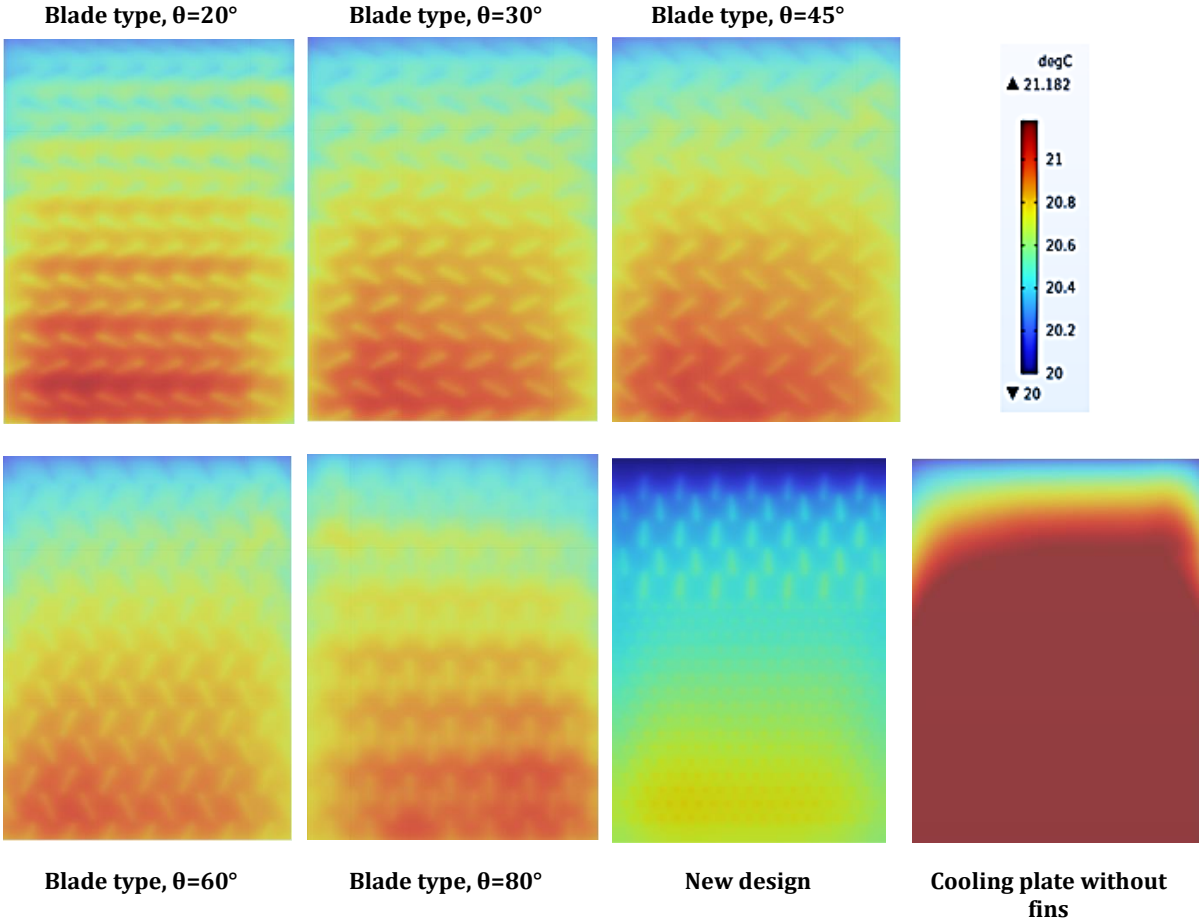

Fig. 8. Comparative thermal performance of different cooling plate configurations visualized through temperature contour maps (temperature scale in °C shown at right). Top row: Blade fins at 20°, 30°, and 45° angles. Bottom row: Blade fins at 60° and 80° angles, pin fins, and no-fin baseline

6.4. Improvement of Design

Figure 8 presents temperature contours of battery surfaces in various cooling plate configurations at a flow rate of 0.6 l/min. The comparative analysis demonstrates that pin fins achieve superior thermal performance with lower maximum temperatures compared to blade geometries, while blade fins with an 80° angle orientation exhibit the lowest pressure drop. This observation suggests an opportunity to optimize cooling performance by combining these complementary advantages into a hybrid design.

To leverage the strengths of both configurations while mitigating their respective limitations, a novel hybrid geometry was developed for the cold plate, incorporating

strategically positioned pin fins and blade fins as illustrated in Figure 2.

This design strategically places blade fins near the inlet region, where the pressure drop is typically highest for pin fins (particularly the 2.5 mm diameter pins), while distributing pin fins throughout other regions to maintain optimal temperature uniformity and maximize heat transfer.

As evidenced in **Fig. 8**, the temperature distribution achieved with this hybrid design closely matches the thermal performance of the optimal 2.5 mm pin fin configuration, demonstrating effective preservation of thermal management capability. Crucially, the pressure drop characteristics show a significant improvement over conventional pin fin designs.

As shown in Fig. **9**, the hybrid design exhibits a pressure drop only about 6 Pa higher than the most hydraulically efficient blade fin configuration (80° angle) at a 0.2 l/min flow rate, while maintaining superior thermal performance. The bar chart in Fig. **9** quantifies pressure drops across all configurations at three different flow rates (0.2, 0.3, and 0.6 l/min). At the highest flow rate of 0.6 l/min, the hybrid design achieved a pressure drop of approximately 245 Pa, significantly lower than pin fin configurations (350-380 Pa for 10 mm and 5 mm pins) and most blade configurations. Only the 80° blade configuration exhibits a slightly lower pressure drop of approximately 205 Pa.

This represents an excellent compromise between thermal and hydraulic performance. Also, the hybrid design exhibits pressure drops that are comparable to those of the models presented in the referenced article. Specifically, at a velocity of 0.2 l/min, the maximum pressure drop for the referenced design [4] is 74.8 Pa. In contrast, the hybrid design shows a pressure drop of 69.45 Pa at the same velocity.

At a higher velocity of 0.3 l/min, the referenced model experiences a maximum pressure drop of 112 Pa, while the hybrid model records a slightly lower pressure drop of 110.02 Pa.

These results indicate that the hybrid design maintains similar performance in terms of pressure drop compared to the original design [4].

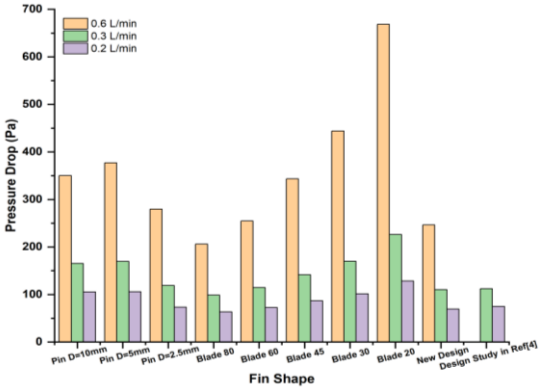

Fig. 9. Pressure drop comparison across different cooling plate configurations at three flow rates (0.6, 0.3, and 0.2 l/min). The chart compares pin fins of varying diameters (10mm, 5mm, 2.5mm), blade fins at different angles (20°-80°), and the novel hybrid design with design study in Ref [4]

Fig. **10** presents a comparative thermal response curve between the current hybrid design and a reference design from previous research [4]. The hybrid design demonstrates superior thermal performance, maintaining the battery at approximately 21.5°C at steady state compared to 22.6°C for the reference design. This is a reduction of approximately 1°C in the maximum battery temperature. This improvement was achieved while reducing aluminum weight by 7% and coolant fluid weight by 66%, along with optimized inlet/outlet configurations. Furthermore, the pressure drop characteristics remain comparable to the reference design at a 0.3 l/min flow rate despite a significant material reduction. These results demonstrate that the strategic integration of different fin geometries can effectively capitalize on their complementary advantages while minimizing their respective limitations. The hybrid design successfully balanced thermal performance, pressure drop, and material efficiency, representing a significant advancement in battery thermal management system optimization.

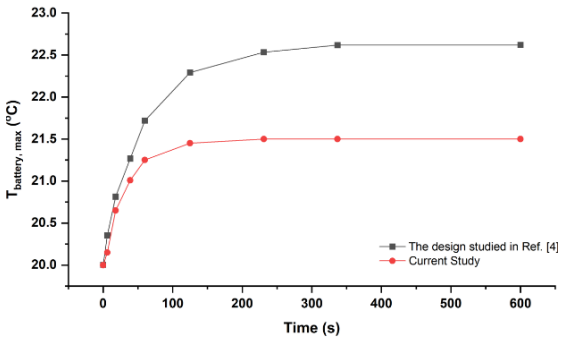

Fig. 10. Transient thermal response comparison between the hybrid fin design (current study) and a reference design from prior research [4]

7. Conclusions and Future Directions

This investigation introduces a groundbreaking hybrid pin-blade fin architecture for lithium-ion battery thermal management systems, fundamentally resolving the traditional thermal-hydraulic performance trade-off that has constrained cooling plate design. Through strategic integration of complementary fin geometries, comprehensive 3D coupled simulations demonstrate exceptional dual optimization capabilities. Some of the major conclusions drawn from the present analysis are:

- The hybrid architecture maintains battery temperatures below 21.5°C during aggressive 5C discharge conditions, a full 1.1°C reduction compared to conventional designs, while simultaneously reducing pressure drop by 30% relative to equivalent pin-fin configurations.
- Utilizing optimized fin geometries in the cooling plate yielded maximum temperature reductions exceeding 2°C compared to fin-less designs, with the hybrid configuration achieving this while requiring only a 246.26 Pa pressure drop at a 0.6 l/min flow rate.
- Quantitative analysis revealed that reducing pin diameters from 10 mm to 2.5 mm decreases maximum battery temperature by 0.3°C, but at the cost of increased pressure drop (approximately 15% higher).
- Blade fin orientation significantly impacts hydraulic performance, with 80° blade fins reducing pressure drop by 65.04 Pa compared to 20° configurations at a 0.2 l/min flow rate. The hybrid design successfully combines the superior thermal performance of 2.5 mm pin fins with the hydraulic efficiency of 80° blade fins, requiring only 6 Pa higher pressure drop than the most hydraulically efficient blade configuration while maintaining equivalent thermal performance to optimal pin arrangements.
- This revolutionary cooling plate architecture achieves these exceptional results while reducing aluminum weight by 7% and coolant volume by 66% compared to benchmark designs, representing a significant advancement in material efficiency.

Future research directions should explore further optimization of hybrid geometries through machine learning algorithms to identify non-intuitive fin distributions that may yield additional performance gains. Investigation of variable-density fin arrangements based on local heat generation patterns within prismatic cells offers promising potential for targeted cooling in high-heat regions. Additionally, experimental validation under dynamic driving cycles and extreme thermal conditions would provide valuable insights into real-world performance. Integration of phase change materials into strategic locations within the hybrid architecture represents another promising direction, potentially enabling further reductions in coolant flow requirements while maintaining thermal stability. Finally, evaluating the manufacturing implications and production scalability of these complex hybrid geometries will be essential for commercial implementation in next-generation electric vehicle battery systems.

Funding Statement

This research did not receive any specific grant from funding agencies in the public, commercial, or not-for-profit sectors.

Conflicts of Interest

The author declares that there is no conflict of interest regarding the publication of this article.

Authors Contribution Statement

Somayeh Jalalichaleshtori : Data Curation; Formal Analysis; Investigation; Resources; Software; Validation; Visualization; Roles/Writing – Original Draft.

Ghanbar Ali Sheikhzadeh : Conceptualization; Methodology; Project administration; Supervision; Roles/Writing – Review & Editing.

References

[1] Abada, S., Marlair, G., Lecocq, A., Petit, M., Sauvant-Moynot, V. & Huet, F., 2016. Safety focused modeling of lithium-ion batteries: A review. *Journal of Power Sources,* 306**,** pp. 178-192.

[2] Alrashdan, A., Mayyas, A. T. & AL-Hallaj, S., 2010. Thermo-mechanical behaviors of the expanded graphite-phase change material matrix used for thermal management of Li-ion battery packs. *Journal of Materials Processing Technology,* 210**,** pp. 174-179.

[3] Cuma, M. U. & Koroglu, T., 2015. A comprehensive review on estimation strategies used in hybrid and battery electric vehicles. *Renewable and Sustainable Energy Reviews,* 42**,** pp. 517-531.

[4] Deng, T., Zhang, G., Ran, Y. & Liu, P., 2019. Thermal performance of lithium ion battery pack by using cold plate. *Applied Thermal Engineering,* 160**,** 114088.

[5] Duan, X. & Naterer, G., 2010. Heat transfer in phase change materials for thermal management of electric vehicle battery modules. *International Journal of Heat and Mass Transfer,* 53**,** pp. 5176-5182.

[6] Hao, H., Geng, Y. & Sarkis, J., 2016. Carbon footprint of global passenger cars: Scenarios through 2050. *Energy,* 101**,** pp. 121-131.

[7] Li, Y., Bai, M., Zhou, Z., Wu, W.-T., Gao, L., Li, Y., Yang, Y., Li, Y. & Song, Y., 2023. Numerical Simulations for Lithium-Ion Battery Pack Cooled by Different Minichannel Cold Plate Arrangements. *International Journal of Energy Research,* 2023**,** 8207527.

[8] Li, Y., Zhou, Z., Hu, L., Bai, M., Gao, L., Li, Y., Liu, X., Li, Y. & Song, Y., 2022. Experimental studies of liquid immersion cooling for 18650 lithium-ion battery under different discharging conditions. *Case Studies in Thermal Engineering,* 34**,** 102034.

[9] Liu, H., Wei, Z., He, W. & Zhao, J., 2017. Thermal issues about Li-ion batteries and recent progress in battery thermal management systems: A review. *Energy conversion and management,* 150**,** pp. 304-330.

[10] Malik, M., Dincer, I., Rosen, M. A., Mathew, M. & Fowler, M., 2018. Thermal and electrical performance evaluations of series connected Li-ion batteries in a pack with liquid cooling. *Applied Thermal Engineering,* 129**,** pp. 472-481.

[11] Mohammed, A. H., Esmaeeli, R., Aliniagerdroudbari, H., Alhadri, M., Hashemi, S. R., Nadkarni, G. & Farhad, S., 2019. Dual-purpose cooling plate for thermal management of prismatic lithium-ion batteries during normal operation and thermal runaway. *Applied Thermal Engineering,* 160**,** 114106.

[12] Monika, K., Chakraborty, C., Roy, S., Dinda, S., Singh, S. A. & Datta, S. P., 2021a. An improved mini-channel based liquid cooling strategy of prismatic LiFePO4 batteries for electric or hybrid vehicles. *Journal of Energy Storage,* 35**,** 102301.

[13] Monika, K., Chakraborty, C., Roy, S., Dinda, S., Sinngh, S. A. & Datta, S. P., 2021b. Parametric investigation to optimize the thermal management of pouch type lithium-ion batteries with mini-channel cold plates. *International Journal of Heat and Mass Transfer,* 164**,** 120568.

[14] Pesaran, A. A., 2002. Battery thermal models for hybrid vehicle simulations. *Journal of power sources,* 110**,** pp. 377-382.

[15] Rabiei, M., GHarehghani, A. & Andwari, A. M., 2023. Enhancement of battery thermal management system using a novel structure of hybrid liquid cold plate. *Applied Thermal Engineering,* 232**,** 121051.

[16] Rao, Z. & Zhang, X., 2019. Investigation on thermal management performance of wedge-shaped microchannels for rectangular Li-ion batteries. *International Journal of Energy Research,* 43**,** pp. 3876-3890.

[17] Sabbah, R., Kizilel, R., Selman, J. & AL-Hallaj, S., 2008. Active (air-cooled) vs. passive (phase change material) thermal management of high power lithium-ion packs: Limitation of temperature rise and uniformity of temperature distribution. *Journal of power sources,* 182**,** pp. 630-638.

[18] Saha, S., Bose, B., Garg, A., Chandra, K. P., Zhao, J., Panda, B. & Gao, L., 2024. A topology optimization for design of double input-single output battery module liquid cooling plate with improved thermal performance. *Journal of Energy Storage,* 97**,** 112750.

[19] Sevilgen, G., Dursun, H. & Kılıc, M., 2023. Experimental and numerical investigations on the thermal performance of three different cold plates designed for the electrical vehicle battery module. *Sustainability,* 15**,** 14162.

[20] Sheng, L., Su, L., Zhang, H., Li, K., Fang, Y., Ye, W. & Fang, Y., 2019. Numerical investigation on a lithium ion battery thermal management utilizing a serpentine-channel liquid cooling plate exchanger. *International Journal of Heat and Mass Transfer,* 141**,** pp. 658-668.

[21] Sun, R., Lu, K. & Cheng, J., 2023. Performance study of battery thermal management system with a bionic cooling plate based on leaf vein channels of plantain. *Journal of Thermal Science and Engineering Applications,* 15**,** 121003-1.

[22] Wang, J., Gan, Y., Liang, J., Tan, M. & Li, Y., 2019. Sensitivity analysis of factors influencing a heat pipe-based thermal management system for a battery module with cylindrical cells. *Applied Thermal Engineering,* 151**,** pp. 475-485.

[23] Wang, Q., Ping, P., Zhao, X., Chu, G., Sun, J. & Chen, C., 2012. Thermal runaway caused fire and explosion of lithium ion battery. *Journal of power sources,* 208**,** pp. 210-224.

[24] Wang, T., Tseng, K., Zhao, J. & Wei, Z., 2014. Thermal investigation of lithium-ion battery module with different cell arrangement

structures and forced air-cooling strategies. *Applied energy,* 134**,** pp. 229-238.

[25] Wu, C., Ni, J., Shi, X. & Huang, R., 2024. A new design of cooling plate for liquid-cooled battery thermal management system with variable heat transfer path. *Applied Thermal Engineering,* 239**,** 122107.

[26] Wu, W., Wang, S., Wu, W., Chen, K., Hong, S. & Lai, Y., 2019. A critical review of battery thermal performance and liquid based battery thermal management. *Energy conversion and management,* 182**,** pp. 262-281.

[27] Zhan, S., Liang, L., Li, Z., Yu, C. & Wang, F., 2024. Topology optimization of liquid cooling plate for lithium battery heat dissipation based on a bionic leaf-vein structure. *International Journal of Heat and Mass Transfer,* 231**,** 125898.

[28] Zhong, Q., Chanra, P. K., Li, W., Gao, L., Garg, A., Lv, S. & Tai, K., 2024. A comprehensive numerical study based on topology optimization for cooling plates thermal design of battery packs. *Applied Thermal Engineering,* 236**,** 121918.

[29] Zhu, J., Wang, J., Cheng, D., Mao, J. & Zhang, K., 2024. Numerical investigation and parameter optimization on a rib-grooved liquid-cooled plate for lithium battery thermal management system. *Journal of Energy Storage,* 85**,** 111085.